RESEARCH ARTICLE

Applied Polymer SCIENCE **WILEY**

High-performance polybenzimidazole blend membranes based on a commercially available anion-exchange polymer and F$_6$PBI for vanadium redox flow batteries

Julian Stonawski[1,2] | **Melanie Schroeder**[3] | **Janett Gördes**[3] | **Linus Hager**[1,2] | **Andreas Hutzler**[1] | **Thomas Böhm**[1] | **Simon Thiele**[1,2] | **Jochen Kerres**[1,4]

[1]Forschungszentrum Jülich GmbH, Helmholtz Institute Erlangen-Nürnberg for Renewable Energy (IET-2), Erlangen, Germany

[2]Department of Chemical and Biological Engineering, Friedrich-Alexander-Universität Erlangen-Nürnberg, Erlangen, Germany

[3]J. Schmalz GmbH, Glatten, Germany

[4]Faculty of Natural Science, North-West University, Potchefstroom, South Africa

Correspondence
Julian Stonawski, Forschungszentrum Jülich GmbH, Helmholtz-Institute Erlangen-Nürnberg for Renewable Energy (IET-2) 91058 Erlangen, Germany.
Email: j.stonawski@fz-juelich.de; stonawski.julian@web.de

Abstract

Renewable energy is essential for the transition to a carbon-neutral society. Due to their intermittent nature, temporary storage is required. The all-vanadium redox flow battery (VRFB) is a promising technology for this purpose. Commercially available membranes, such as the FAPQ330 from Fumatech BWT, already show reasonable performance but still have room for improvement in selectivity and conductivity. In this study, we developed new ductile porous blend membranes based on the polybenzimidazole F$_6$PBI by mixing it with poly(diallyldimethylammonium bis(trifluoromethane)sulfo-nimide), which was prepared from the commercially available poly(dimethylammonium chloride) (PDADMAC). Three types of membranes with different amounts of PDADMA*TFSI in the blend solution were prepared and characterized. Ex-situ conductivity measurements showed conductivities between 8.3 and 30.5 mS cm^{-1}. Ex-situ permeability tests revealed significantly lower permeabilities compared to the reference membrane FAPQ330. No change in ex-situ conductivity was measured after the ex-situ stability test. F$_6$PBI-PDAD37 reached the highest energy efficiency at 50, 100, and 200 mA cm^{-2} among all tested membranes. For example, a VRFB single-cell equipped with F$_6$PBI-PDAD37 showed an improved EE of 76.5% at 200 mA cm^{-2}, which is higher than the EE of FAPQ330 (74.3%).

KEYWORDS
blend membranes, ion-conducting polymers, poly(diallyldimethylammonium chloride), polybenzimidazole, vanadium redox flow batteries

1 | INTRODUCTION

Climate change and associated environmental impacts have become a primary societal concern. Programs like the European Green Deal are trying to mitigate these impacts by reducing emissions and heading towards a climate-neutral continent.[1] Renewable energies such as wind and solar energy are vital in this transformation. Compared to fossil fuels, the fluctuating nature of these resources can lead to issues such as load peaks or voltage

fluctuations. Therefore, it is necessary to store the energy to encounter these challenges.[2,3] The all-vanadium redox flow battery (VRFB) is a promising energy storage technology. Long-term stability, the decoupling of power and capacity, and high energy efficiency have raised interest in this technology.[4–6] One of the key materials in such a system is the membrane, which separates the two half-cells of the battery. Cation exchange membranes (CEM), anion exchange membranes (AEM), free amine-based membranes, or combinations of these can be used.[7–10] To ensure long-term stability and high battery efficiencies, these materials need high ionic conductivity, high perms-electivity among transported species, and superior chemical stability, especially versus the oxidizing V(V) species.[11–14]

In recent years, research for VRFB membranes focused on new materials with improved ionic conductivity and selectivity. For example, Gigli et al. used sulfonated poly(phenylene sulfide sulfone) as a membrane material, which showed reasonable voltage efficiency (VE) and coulomb efficiency (CE). However, sulfonated materials generally show significant vanadium crossover and, as a result, lower CE compared to AEMs or free amine-based membranes.[15,16]

Polybenzimidazoles (PBI) are widely considered an alternative to sulfonated materials due to their superior mechanical and crossover mitigating properties. Gubler et al. showed that this leads to CEs >99% at low current densities when thin PBI membranes with a thickness of down to 10 μm are used in a VRFB single cell.[17] The basic benzimidazole groups within the main chain absorb acids, i.e. sulfuric acid, thus leading to ionic conductivity in acidic media. However, as the conductivity is relatively low, the applicability of pure PBI in VRFB is limited.[18–21] Different approaches to increase the conductivity of pure PBIs have been investigated. Tang et al. attached long quaternary ammonium side chains onto meta-polybenzimidazole (m-PBI), leading to a hybrid material capable of absorbing sulfuric acid through the remaining benzimidazole moieties and conducting anions due to the quaternary ammonium groups.[22] Another approach is the pre-treatment of PBI membranes with different solutions. By pre-treating m-PBI with 15 M phosphoric acid and subsequent doping in sulfuric acid to replace the excess phosphoric acid, it was possible to increase the proton conductivity from 1.6 to 17.3 mS cm^{-1}, which the authors of that study assumed to be due to an irreversible increase in sulfuric acid uptake.[23] Besides these approaches, Jung et al. investigated mixing m-PBI and an anion exchange polymer, FAA3, by FUMATECH BWT GmbH. Adding the anion exchange polymer increased the conductivity and improved the VE and energy efficiency (EE) in a VRFB single-cell test. The concentration

of the absorbed sulfuric acid inside the membrane was determined after placing the membranes in aqueous sulfuric acid solutions with different concentrations. It was shown that the concentration within the membrane decreases with an increasing amount of FAA3 from 8.8 M for the pure m-PBI to 6.1 M for the membrane with 33 wt% FAA3 when immersed in 2 M sulfuric acid. Because quaternary ammonium-containing polymers tend to bind more water, the sulfuric acid inside the membrane is diluted. Darling et al. found that sulfuric acid has a maximum conductivity at a concentration of around 3–4 M, which explains the increased conductivity with concentrations approaching this maximum.[24] A single cell equipped with such a membrane led to an EE of 86% at 80 mA cm^{-2}. Stability tests in 1.5 M VO$_2^+$ showed an increasing amount of V(IV) after 87 days for membranes with higher amounts of FAA3, most probably due to a degradation of the FAA3 polymer. As the chemical structure of the polymer is unknown, it is difficult to determine the reason for this degradation.[25]

In this study, we applied the abovementioned approach of mixing a PBI with an anion-conducting polymer to a novel polymer system. Poly(diallyldimethylammonium chloride) (PDADMAC) was chosen as the anion exchange material due to its commercial availability and chemical stability in the VRFB.[26–31] Solubility in polar-aprotic solvents is necessary to blend a polymer with a polybenzimidazole. Therefore, an ion exchange process was used to achieve solubility in dimethyl sulfoxide (DMSO), N-methyl-2-pyrrolidone (NMP), and N,N-dimethylacetamide (DMAc).[32] Hexafluoropropylidene polybenzimidazole (F$_6$PBI) was chosen as the polybenzimidazole component due to its superior solubility, stability, and mechanical properties.[33,34] The resulting blend membranes are characterized in terms of swelling properties, mechanical properties, conductivity, V(IV) crossover, and stability in V(V) electrolyte. In addition to ex-situ measurements, in-situ VRFB single-cell tests at different current densities are presented.

2 | RESULTS AND DISCUSSION

2.1 | Preparation and ex-situ characterization of PDADMAC/F$_6$PBI blend membranes

PBIs have superior crossover mitigation properties towards the vanadium species but low ionic conductivities. Thus, a method to improve the conductivity was necessary. One approach to modifying the properties of PBIs is blending them with an anion-exchange polymer.[25] Due to stability and economic reasons, a commercially
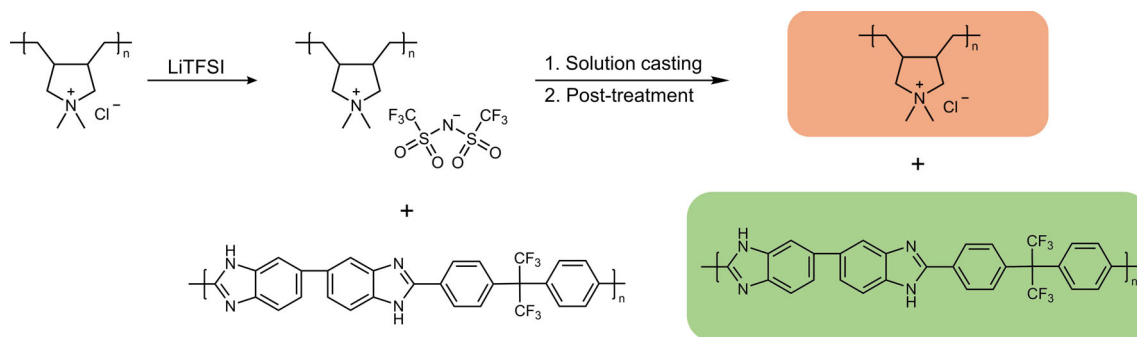
FIGURE 1 Schematic representation of the PDADMAC/F$_6$PBI blend membranes fabrication process. [Color figure can be viewed at wileyonlinelibrary.com]

available and quaternary ammonium group-containing polymer, PDADMAC, was selected.[30,35] PDADMAC is not soluble in organic polar aprotic solvents where F$_6$PBI is soluble, i.e. DMSO, NMP, or DMAc. According to the literature, the solubility properties of PDADMAC can be altered towards solubility in aprotic polar solvents by exchanging the chloride counterion with a more hydrophobic ion.[32,36–38]

TFSI$^-$-exchanged PDADMAC was selected because it has the most favorable properties in terms of solubility and miscibility with F$_6$PBI and was therefore used to prepare the blends. A schematic representation of the fabrication process of the PDADMAC/F$_6$PBI blend membranes is shown in Figure 1.

Three different membranes with target PDADMAC contents of 21, 28, and 37 wt% were produced using the solution casting method. In all cases, ductile membranes were received with dry thicknesses between 14 and 18 μm. The membranes were analyzed for residual TFSI$^-$-counterions by ^{19}F-NMR. Only minor amounts of residual TFSI$^-$ were found. The percentage of residual TFSI$^-$ counterions based on the initially present amounts are given in Table S1. In all cases, the remaining amount was below 2% of the initially present TFSI$^-$.

For reference, pure F$_6$PBI and a commercially available membrane, FAPQ330 (FUMATECH BWT GmbH), were analyzed in addition to the blend membranes. The morphology of the membranes was investigated by acquiring HAADF-STEM images of the membrane's cross sections. As shown in Figure S1, all membranes showed porosity with increasing pore sizes at rising PDADMA*TFSI contents in the blend solution. This observation most likely results from a partial phase separation between the F$_6$PBI and the PDADMA*TFSI, resulting in a two-phase system with distinct nanophases of PDADMA*TFSI. During the ion exchange procedure, the TFSI$^-$ is replaced by Cl$^-$ counterions, thus forming water-soluble PDADMAC. As was shown in other systems, the initial hypothesis was that the entanglement of the two

high-molecular-weight polymers is strong enough to prevent the washing-out of the water-soluble PDADMAC.[39] However, reduced entanglement is present within the nanophases of pure PDADMAC, allowing the PDADMAC to be washed out during the post-treatment, thus creating porosity.[40] The composition of the remaining continuous phase was further analyzed via Mohr's titration to investigate if all or only a part of the PDADMAC was removed from the membranes. As shown in Table 1, all prepared membranes still contained a considerable amount of PDADMAC, supporting the abovementioned hypothesis. Therefore, it can be concluded that the addition of PDADMAC to F$_6$PBI leads to the formation of both a continuous mixed phase, in which the PDADMAC is prevented from being washed out due to the entanglement of the polymer chains and distinct PDADMAC nanophases. With increasing amounts of PDADMAC, the portion of PDADMAC in the continuous phase and the size of the PDADMAC nanophases increases, which leads to bigger pores and increased porosity of the post-treated blend membranes.

Another crucial property of acid-doped membranes is the acid uptake and the ADL.[41,42] Table 1 shows that an increasing amount of PDADMAC added to the blend solution led to an increased acid uptake and a significant increase in thickness when immersed in 2 M H$_2$SO$_4$.

However, besides the amount of the absorbed solution, the acid concentration within the membrane must also be considered. For pure PBI membranes, it is significantly higher than in the surrounding solution.[41,43] As shown in Figure 2, titrations yielded an acid concentration of 7.8 mol L^{-1} for pure F$_6$PBI when placed in 2 M H$_2$SO$_4$, corresponding to an ADL of 1.4.

Darling et al. observed that the conductivity of sulfuric acid is strongly related to its concentration.[24] The maximum conductivity is reached at about 30 wt%, corresponding to a concentration of about 3.7 mol L^{-1}. Therefore, it was assumed that the high concentration of the absorbed acid and the several H-bridges between the

TABLE 1 Overview of F_6PBI/poly(dimethylammonium chloride) (PDADMAC) blend membrane composition and their acid swelling properties.

Membrane	wt% PDADMAC theor. (%)	wt% PDADMAC titrated (%)	P%[a] (%)	AU[b] (%)	AS[c] (%)	ADL[d]
FAPQ330	–	–	–	30 ± 3	18 ± 9	–
F_6PBI	0	–	–	47 ± 2	17 ± 1	1.40 ± 0.02
F_6PBI-PDAD21	21	15.3 ± 0.2	6.8 ± 0.2	68 ± 5	17 ± 1	1.50 ± 0.05
F_6PBI-PDAD28	28	17.0 ± 1.0	13.2 ± 1.1	85 ± 1	30 ± 12	1.92 ± 0.09
F_6PBI-PDAD37	37	22.1 ± 0.4	19.2 ± 0.5	120 ± 8	87 ± 7	2.33 ± 0.02

[a]Weight fraction of voids assuming they are filled.

[b]In 2 M H_2SO_4 for 48 h at RT.

[c]Change in thickness after immersion in 2 M H_2SO_4 for 48 h at RT.

[d]Moles of H_2SO_4 per benzimidazole unit.
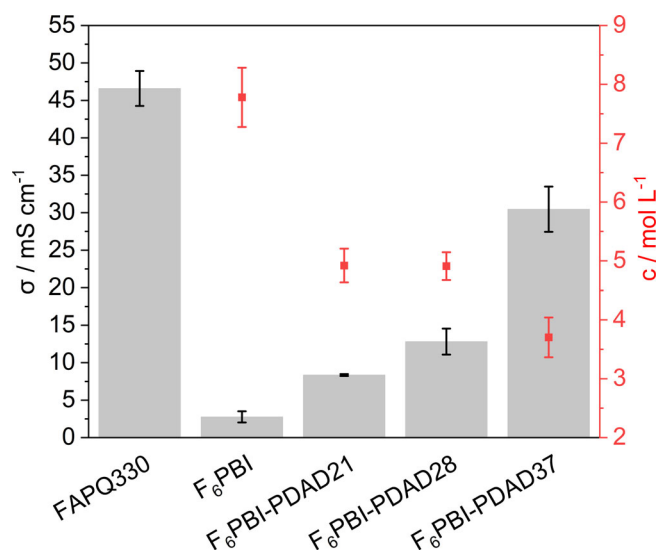
FIGURE 2 Conductivity σ in 0.5 M H_2SO_4 and titrated H_2SO_4 concentration c of the reference and blend membranes. [Color figure can be viewed at wileyonlinelibrary.com]

benzimidazole units led to an unusually low conductivity despite the high ion exchange capacity (IEC) of 3.7 mol g^{-1}.[18] Jung et al. have previously shown that adding an anion exchange polymer to a polybenzimidazole polymer increases the total acid uptake and decreases the concentration of the absorbed acid.[25] Table 1 and Figure 2 show that this is also true for the PDADMAC/F_6PBI system. The addition of 21 wt% PDADMA*TFSI to the blend reduces the acid concentration from 7.8 mol L^{-1} for pure F_6PBI to 4.9 mol L^{-1} and increases the acid uptake from 47% to 68%. For the membranes F_6PBI-PDAD28 and F_6PBI-PDAD37, the acid uptake increases to 85% and 120%, and the acid concentration decreases to 4.9 and 3.7 mol L^{-1}, respectively. This observation can be explained by three different effects. First, the increasing amount of PDADMAC in the continuous phase leads to an increased water uptake due to the hydrophilicity of PDADMAC. Second, the increasing

porosity additionally increases the uptake of the surrounding sulfuric acid as the pores are filled. Third, the lower amount of polybenzimidazole decreases the amount of benzimidazole groups available for protonation, thus diminishing the uptake of sulfuric acid. The combination of these three effects leads to an overall increase in water and acid uptake with increasing amounts of PDADMA*TFSI added to the blend. Additionally, more water is absorbed relative to sulfuric acid, leading to decreased acid concentration, thereby approaching the conductivity maximum at a sulfuric acid concentration of 3.7 mol L^{-1}.[24,41]

The conductivity of the membrane plays an important role in the performance of the cell. Therefore, the conductivity of the novel membranes and the reference membrane FAPQ330 were measured in 0.5 M H_2SO_4, and the corresponding results are shown in Figure 2. As can be seen, the pure F_6PBI showed a conductivity of 3 mS cm^{-1}, which means high ionic resistance and low voltage efficiency when used as a membrane in a vanadium redox flow battery. Increasing amounts of PDADMA*TFSI into the blend solution led to rising ex-situ conductivities, which can be attributed to a combination of two effects: An increase in the overall acid uptake and the decreasing sulfuric acid concentration inside the membrane, thereby approaching the concentration with the maximum conductivity of sulfuric acid at 3.7 mol L^{-1}. The comparably low conductivity increase, when going from 21% to 28% PDADMA*TFSI to the blend solution, can be explained by the fact that the acid concentration does not change due to the comparable composition of the continuous phase (compare Table 1). For this step, the rise in conductivity is primarily the result of the increased overall acid uptake due to the increased porosity. However, adding 37% PDADMA*TFSI to the blend solution led to a steeper increase in conductivity to 30 mS cm-1, resulting from higher overall sulfuric acid uptake and decreased acid
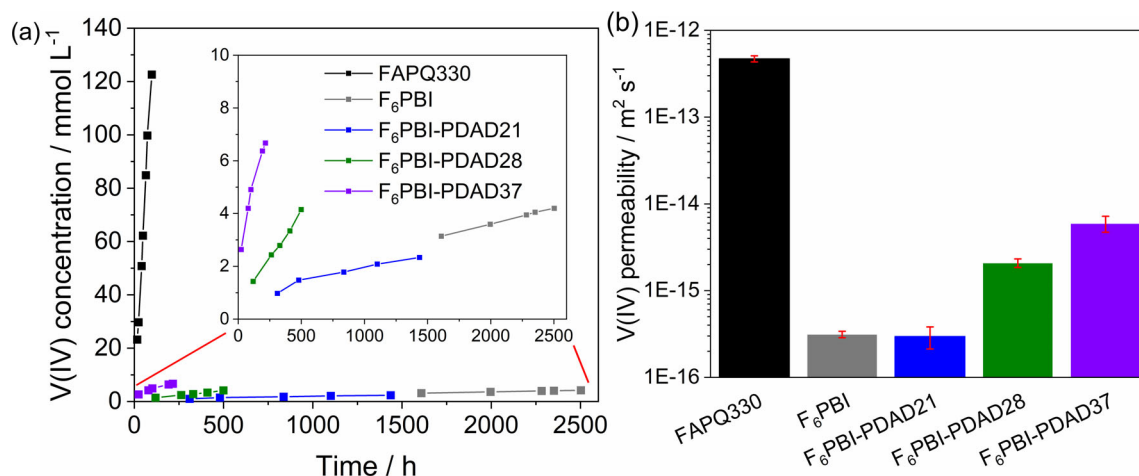
FIGURE 3 Results of the ex-situ permeability tests. (a) Change of the V(IV) concentration over time. (b) Ex-situ V(IV) permeability of the tested blend membranes. [Color figure can be viewed at wileyonlinelibrary.com]

concentration of 3.7 mol L^{-1}. All conductivities of the prepared membranes are lower than the 47 mS cm^{-1} of the FAPQ330. However, even at low film thicknesses, polybenzimidazoles have superior crossover mitigation properties for vanadium species, allowing the utilization of thin membranes with decreased area resistances without sacrificing much CE.[44]

In addition to conductivity, the membrane permeability of vanadium species is another parameter that affects the performance of a VRFB cell. Therefore, VRFB membrane design aims to enhance proton conductivity and permselectivity between vanadium species and protons. Polybenzimidazoles are known to have low vanadium crossover, resulting in a high H$^+$/V permselectivity. Therefore, the aim was to increase the conductivity while maintaining the low crossover and the high selectivity. The permeability of V(IV) through the membrane can be observed by placing a membrane into an H-cell between MgSO$_4$/H$_2$SO$_4$ and VOSO$_4$/H$_2$SO$_4$ solutions with the same concentrations. The V(IV) concentration is monitored on the MgSO$_4$ side over time. From these data, the V(IV) permeability can be calculated.[45,46] Figure 3 shows the evaluated data for the PDADMAC/F$_6$PBI blend membranes.

All novel membranes exhibited significantly lower V(IV) permeabilities than the commercial membrane due to the exceptionally high selectivity of polybenzimidazoles resulting from the dense hydrogen bonding network between the benzimidazole units. This network leads to narrow ion-conducting channels of the blend membranes, which are supposed to be below 0.7 nm to prevent an excessive crossover of hydrated vanadium species.[47] Increasing PDADMA*TFSI contents in the blend solutions raised the V(IV) permeability from 3.1×10^{-16} m^2 s^{-1} for pure F$_6$PBI to 6.0×10^{-15} m^2 s^{-1}

for F$_6$PBI-PDAD37. This increase is attributed to increased overall acid uptake and porosity with greater amounts of PDADMA*TFSI added to the blend solution. The higher acid uptake enlarges the diameter of the ion exchange channel, facilitating the passage of all moving species, whereby the increased porosity decreases the effective membrane thickness the ionic species need to traverse.[47] Despite the slightly decreasing V(IV) permeability, the blend membranes maintained substantially lower V(IV) permeability than the commercial reference membrane. This result highlights the effectiveness of the blend approach in maintaining reasonable crossover characteristics while simultaneously enhancing the conductivity of the membranes, thereby improving the overall membrane performance.

To evaluate the stability of the membranes in an acidic V(V) solution, pieces of the membranes were immersed in 1.6 M V(V)/2 M H$_2$SO$_4$ solution for 820 h. The solutions for V(IV) were analyzed after the test. In addition, the conductivity of the membranes was analyzed in 0.5 M H$_2$SO$_4$ before and after the test. The results are shown in Figure 4.

In all cases, the membranes showed no disintegration after the ex-situ aging test. V(IV) formation is assumed to result from a reaction between V(V) and the polymers. Amounts of V(IV) per gram of polymer between 0.5 and 1.2 mmol g^{-1} were found (Figure 4a). For the novel membranes, slightly higher amounts of V(IV) per gram polymer were measured compared to the reference membrane FAPQ330. The greatest amounts of V(IV) were found for F$_6$PBI-PDAD28 and F$_6$PBI-PDAD37, eventually resulting from the higher overall acid uptake. This probably leads to higher concentrations of V(V) within the ion-conducting channels and, therefore, to an increased reaction rate between the V(V) species and the polymer
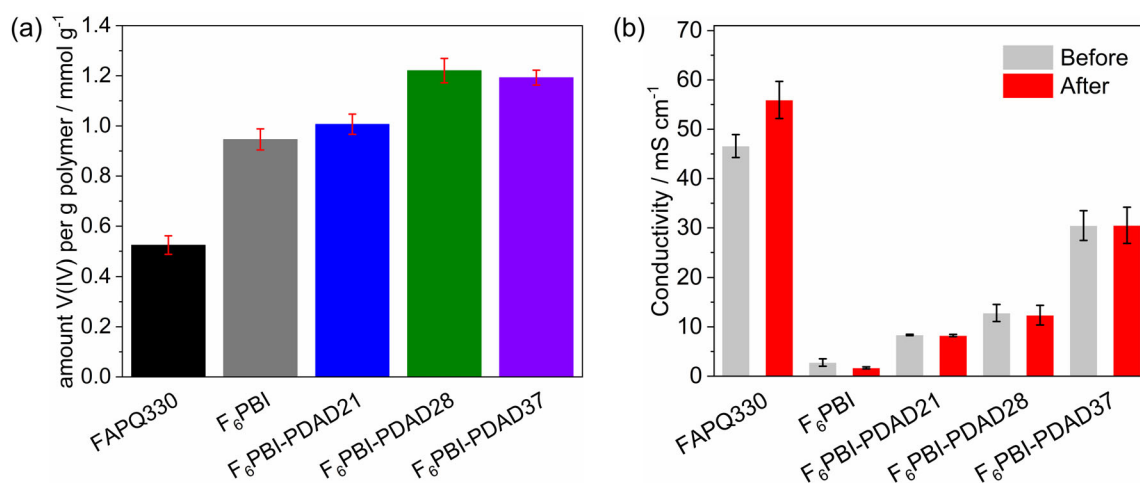
FIGURE 4 Results of the stability test in 1.6 M V(V)/2 M H_2SO_4 solution for 820 h. (a) Amount of V(IV) per gram polymer in the stability solution. (b) Conductivity in 0.5 M H_2SO_4 of the membranes before and after the stability test. [Color figure can be viewed at wileyonlinelibrary.com]

TABLE 2 Tensile properties of the dry membranes at 23°C and 25% relative humidity.

Polymer	Tensile strength (MPa)	Young's modulus (MPa)	Elongation at break (%)
FAPQ330	35.1 ± 0.8	422.4 ± 156.9	57.9 ± 23.9
F_6PBI	114.4 ± 4.8	2627.0 ± 362.9	5.1 ± 0.7
F_6PBI-PDAD21	85.7 ± 4.9	2063.5 ± 369.7	8.8 ± 3.0
F_6PBI-PDAD28	77.3 ± 1.7	2034.6 ± 508.8	8.7 ± 1.6
F_6PBI-PDAD37	58.2 ± 5.3	1527.1 ± 407.5	5.5 ± 2.8

structures. However, no significant change in ex-situ conductivity was measured after the ex-situ aging experiment except for the FAPQ330 (Figure 4b). Interestingly, the conductivity of the FAPQ330 increased after the cell test, which could result from a change in microstructure due to the penetration of V species into the membrane. Therefore, based on the unchanged conductivity and intactness of the membranes after the stability test, we consider the novel membranes to be stable under the tested conditions.

Tensile tests with dry membrane pieces were performed to analyze the effect of the PDADMAC amount within the blend on the mechanical properties. The results are presented in Table 2.

Adding PDADMAC decreased the tensile strength and Young's modulus compared to the pristine F_6PBI. For example, adding 37% PDADMAC decreased the tensile strength from 114.4 MPa for pure F_6PBI to 58.2 MPa and the Young's modulus from 2627.0 to 1527.1 MPa. The addition of PDADMAC had no significant effect on the elongation at break. The decline in tensile properties is primarily attributed to two different effects. First, PDADMAC is a brittle and highly charged material. As

polybenzimidazoles are known for their excellent mechanical properties, a worsening of the tensile strength and Young's modulus with increasing amounts of PDADMAC in the continuous phase can be expected.[48] Second, the membranes exhibit increased porosity with higher amounts of PDADMA*TFSI in the blend solution, further compromising their tensile properties.[49] Compared to the reference membrane FAPQ330, the novel membranes showed higher Young's moduli and tensile strength, mainly due to the superior mechanical properties of polybenzimidazoles.[50]

2.2 | In-situ VRFB single-cell tests

To test the membranes electrochemically, 10 cc cycles with 50 mA cm^{-2}, 10 cc cycles with 100 mA cm^{-2}, and 10 cc cycles with 200 mA cm^{-2} from SOC 20%–80% were performed with single-cells equipped with F_6PBI, F_6PBI-PDAD21, F_6PBI-PDAD28, and F_6PBI-PDAD37. For comparison, the same test was performed with the FAPQ330. The results of the membranes are shown in Figure 5.
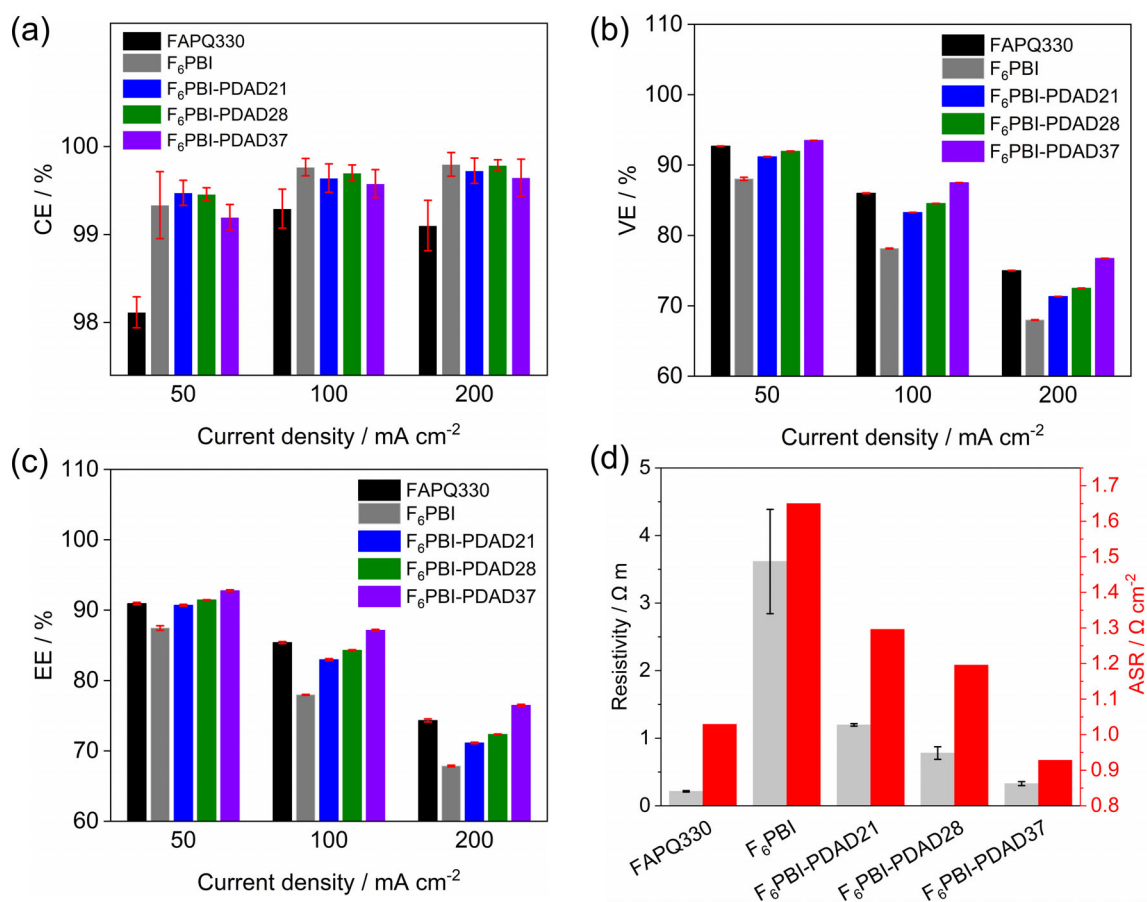
FIGURE 5 VRFB single-cell performance data of FAPQ330 and different in-house prepared F_6PBI (blend) membranes. (a) CE, (b) VE, (c) EE at 50, 100, and 200 mA cm^{-2}; (d) Correlation of ASR measured at SOC 50% and ex-situ resistivity in 0.5 M H_2SO_4. Efficiencies are the mean value of the last five cycles at each current density. [Color figure can be viewed at wileyonlinelibrary.com]
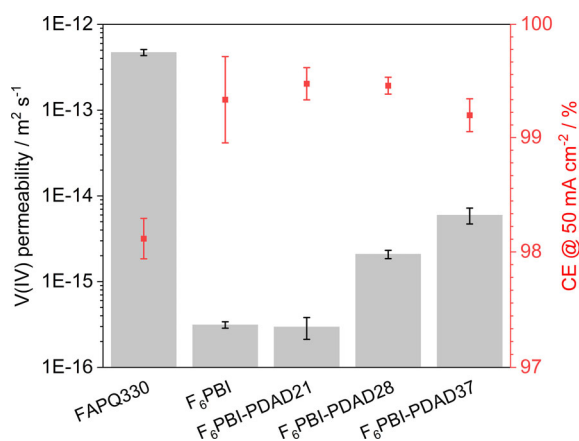

FIGURE 6 Ex-situ V(IV)-permeability versus CE at 50 mA cm^{-2} for the tested membranes. [Color figure can be viewed at wileyonlinelibrary.com]

As shown in Figure 5 and Figures S2–S4, all membranes were suitable for cycling in a VRFB single-cell test. Generally, the length of a single cycle influences the CE of a VRFB cell equipped with a specific membrane.

The lower the current density and the higher the SOC range, the longer the cycle and the lower the CE. Therefore, the CEs were compared at the lowest measured current density of 50 mA cm^{-2}. Figure 5a shows the measured CE when cycled with 50 mA cm^{-2} for the five membranes. All membranes showed significantly higher CEs than the FAPQ330, even though the dry thicknesses were approximately 50% less than that of the FAPQ330. All CEs of the novel membranes are above 99%, corresponding to the high selectivity of these membranes. In addition to other loss mechanisms, the crossover of V species across the membrane during cycling significantly affects the CE. Therefore, the permeability determined with the static crossover test can be correlated with the CE, as shown in Figure 6.

The comparison of the CE and the permeabilities in Figure 6 shows that the membrane with the highest ex-situ permeability, the FAPQ330, also has the lowest CE in a single cell at a current density of 50 mA cm^{-2}. The slightly lower CE of F_6PBI-PDAD37 (99.2%) compared to F_6PBI-PDAD21 and F_6PBI-PDAD28 (99.5%) at

50 mA cm^{-2} can be attributed to an increased V(IV) permeability. This is probably the result of the increased membrane swelling, leading to a higher diameter of the ion-conducting channels. Previous studies showed that V crossover increases significantly when the channel size exceeds the size of the hydrated V species, which is about 0.7 nm.[47] Furthermore, the more pronounced porosity decreases the real membrane thickness that charge carriers need to pass through, thereby facilitating the crossover of all species and negatively impacting the CE.[20]

In general, membrane thinning leads to increased V crossover and, therefore, reduces the CE but also improves the VE due to the lower resistance of the cell. For the pure F$_6$PBI and F$_6$PBI/PDADMAC blend membranes, the CE is above 99%, and the membrane thickness is lower than that of FAPQ330. The high selectivity and good mechanical properties of these membranes facilitate the application of thin membranes with improved VE. However, despite the lower thicknesses of F$_6$PBI, F$_6$PBI-PDAD21, and F$_6$PBI-PDAD28, the VEs are still below that of the FAPQ330 due to the low conductivity (compare Figure 5b). In contrast, the cell equipped with F$_6$PBI-PDAD37 reached a higher VE than the FAPQ330, resulting from the high conductivity of 30.5 mS cm^{-1} and low membrane thickness of 14 μm. Figure 5d clearly shows the correlation between the ex-situ resistivity in 0.5 M H$_2$SO$_4$ and the in-situ measured area specific resistance (ASR). With decreasing ex-situ resistivity, a clear trend to lower ASRs was observable, thus allowing the estimation of the in-cell VE via a parameter measured ex-situ. For F$_6$PBI-PDAD37, a significantly lower ASR was observed, which is the combined result of the relatively high conductivity and the small thickness of 14 μm. At low current densities, F$_6$PBI-PDAD21 and F$_6$PBI-PDAD28 showed EE comparable to that of the FAPQ330, while at higher current densities, the EE was below that of the FAPQ330 due to the lower VE (compare Figure 5c). The high selectivity of F$_6$PBI-PDAD37 coupled with high conductivity resulted in the highest EE for all measured membranes at all tested current densities. We, therefore, conclude that F$_6$PBI-PDAD37 showed the best in-situ performance among all novel developed membranes.

3 | CONCLUSION

In this study, F$_6$PBI-based membranes were developed by blending F$_6$PBI with an anion exchange polymer PDADMA*TFSI prepared from the commercially available PDADMAC. STEM images revealed increasing porosity and PDADMAC contents in the remaining continuous phase with higher amounts of PDADMA*TFSI in the blend solution. The membranes exhibited an increased total sulfuric acid uptake and a decreased sulfuric acid concentration, resulting in an improved conductivity compared to pure F$_6$PBI. The V(IV) permeabilities were significantly lower than that of FAPQ330 and increased with increasing amounts of PDADMA*TFSI in the blend solution. Tensile tests showed decreasing tensile properties with increasing PDADMAC content. However, all prepared membranes were ductile and flexible due to the superior mechanical properties of F$_6$PBI. Single-cell VRFB tests showed increased CEs compared to the commercial reference membrane FAPQ330. VEs were lower for F$_6$PBI-PDAD21 and F$_6$PBI-PDAD28 but higher for F$_6$PBI-PDAD37. The EE of F$_6$PBI-PDAD37 was significantly higher than that of FAPQ330 at all current densities tested. After ex-situ stability tests in 1.6 M V(V)/2 M H$_2$SO$_4$ solution, all membranes were intact, and no change in the ex-situ conductivity was measurable, demonstrating the stability of newly developed membranes within the tested conditions. Due to the ease of preparation, high VRFB performance, and stability of the materials, the presented system can be considered an efficient membrane system for VRFBs.

4 | EXPERIMENTAL SECTION

4.1 | Materials

Poly(diallyldimethylammonium chloride) solution (M$_w$ 400,000–500,000 g mol^{-1}; 20 wt% in H$_2$O), bis(trifluoromethane)sulfonimide lithium salt (LiTFSI), N,N-dimethylacetamide, magnesium sulfate and hydrochloric acid 37% were purchased from Sigma Aldrich. Vanadyl(IV) oxide sulfate hydrate was purchased at TCI Deutschland GmbH. The polybenzimidazole F$_6$PBI was purchased from Yanjin Technology. FAPQ330 membranes were provided by FUMATECH BWT GmbH. The vanadium electrolyte (1.6 M V(III/IV) in 2 M H$_2$SO$_4$) was purchased from GfE Metalle und Materialien GmbH. The thermally activated carbon felts (SIGRACELL® GFD 4.65 EA) were provided by SGL CARBON GmbH. All chemicals and materials were used without further purification.

4.2 | Preparation of poly(diallyldimethylammonium bis(trifluoromethane)sulfonimide

The ion exchange of PDADMAC with the respective counterions was performed by adding an aqueous solution of the respective salt to an aqueous solution of PDADMAC.

The following procedure describes the preparation of poly(diallyldimethylammonium bis(trifluoromethane)sulfonimide) (PDADMA*TFSI). An aqueous 20 wt% PDADMAC solution (119 g, 147 mmol, 1.00 eq) was placed in a 2 L beaker with 1200 mL of deionized water (DI water) and a stirring bar. LiTFSI (50.8 g, 177 mmol, 1.10 eq.) was dissolved in 120 mL DI water. The LiTFSI solution was added to the PDADMAC solution, and the resulting suspension was allowed to stir for 2 h at room temperature (RT). The precipitate was filtered off, washed 5x with fresh DI water, and dried at 85°C for 24 h.

4.3 | Preparation of PDADMAC/F_6PBI blend membranes

The membranes were produced by using the solution casting method. The following procedure describes the preparation of the PDADMAC/F_6PBI blend membrane with 28 wt% PDADMAC. 0.96 g PDADMA*TFSI and 5.01 g DMAc were added to 8.58 g of a 7.5 wt% F_6PBI solution in DMAc. The mixture was stirred at RT until homogeneous and was cast on a glass plate with a gap height of 350 μm and dried for 2 h at 140°C. The membrane was detached by immersing the glass plate in DI water. Subsequently, the membrane was post-treated 10 times in 1 M HCl for 24 h at 85°C, 1 time in 1 M K_2CO_3 at 85°C for 24 h, and 1 time in H_2O at 85°C for 24 h. Finally, the membrane was dried at 85°C for 24 h. The resulting membranes were labeled F_6PBI-PDADx, where x is the wt% of PDADMAC in the post-treated membrane. The dry thickness of the membranes was between 14 and 18 μm.

4.4 | Characterization

^{19}F-NMR measurements were performed on a JEOL JNM-ECZ-500R with a proton resonance frequency of 500 MHz at room temperature. Deuterated solvents were used for reference purposes. The analysis of the spectra was performed by using the software MestReNova (V. 14.2.0-26256). The residual amount of $TFSI^-$ $\%TFSI^-$ based on the initially present amount was determined by using the following formula where n_{F_6PBI} is the amount of F_6PBI, $n_{PDADMA*TFSI}$ is the amount of PDADMA*TFSI and I_{TFSI^-} is the integral of the $TFSI^-$ signal when the integral of the F_6PBI signal is set to 100.

$$\%TFSI^- = \frac{n_{F_6PBI}}{n_{PDADMA*TFSI}} \times I_{TFSI^-}. \quad (1)$$

Before acquiring high-angle annular dark field scanning transmission electron microscopy (HAADF-STEM)

images, membrane pieces were immersed three times in 1 M Na_2WO_4 solution for 24 h at RT. Subsequently, the membranes were washed three times with ultrapure water to remove excess Na_2WO_4. Thin slices of the membrane's crosssections were received by embedding membrane pieces in an epoxy resin (Araldite 502) and subsequent cutting with an RMC Boeckeler PowerTome equipped with a Diatome ultra 45 diamond knife, thereby using water as a floating liquid. The images were captured with an acceleration voltage of 200 kV, a beam current of 40 pA, and a convergence angle of 10.5 mrad.

The composition of the membranes was determined by utilizing Mohr's titration. For this, three pieces for each membrane weighing between 30 and 60 mg were washed three times at 85°C with ultrapure water to remove any excess chloride ions present in the membranes and dried for 24 h at 85°C. Afterwards, the pieces were exchanged three times with 25 mL of 1 M $NaNO_3$/0.1 M HNO_3 for 24 h at RT to exchange the Cl^- counterions of the PDADMAC to NO_3^-. After washing with 10 mL ultrapure water at 85°C for 24 h, all solutions that had contact with the membranes were collected and titrated with 0.01 M $AgNO_3$. The weight fraction of PDADMAC $w\%_{PDADMAC}$ in the membrane was calculated by using the following equation, where V_{AgNO_3} is the volume of the consumed $AgNO_3$ solution in L, c_{AgNO_3} is the concentration of the $AgNO_3$ solution in $mol\,L^{-1}$, $M_{PDADMAC}$ is the molecular weight of PDADMAC in $g\,mol^{-1}$ and m_{Mem} is the weight of the membrane piece in g.

$$w\%_{PDADMAC} = \frac{V_{AgNO_3} \times c_{AgNO_3} \times M_{PDADMAC}}{m_{Mem}}. \quad (1)$$

Additionally, the porosity based on the weight fraction of voids, assuming they are filled, was calculated with the following equation, where $w\%_{F_6PBI}$ is the mass fraction of F_6PBI in the blend calculated from the titrated amount of PDADMAC, and $w\%_{PDADMAC,aim}$ and $w\%_{F_6PBI,aim}$ are the initially added mass fractions of PDADMAC and F_6PBI, respectively.

$$P\% = w\%_{PDADMAC,aim} - \frac{w\%_{F_6PBI,aim} \times w\%_{PDADMAC}}{w\%_{F_6PBI}}. \quad (2)$$

Acid uptake, acid swelling, and acid concentration of the membranes were measured by placing membrane pieces into 2 M H_2SO_4 for at least 72 h. The wet pieces were dried by gently blotting with science lab wipes 7557 provided by KIMTECH® and weighed. The thicknesses were measured using the digital micrometer Series 293 from Mitutoyo. The acid uptake ($AU\%$), acid swelling ($AS\%$), and acid doping level (ADL) were calculated with the following equations where m_{wet} is the wet weight, m_{dry} is the dry weight, d_{wet} is the wet thickness,

d_{dry} is the dry thickness, n_{BI} is the molar quantity of benzimidazole molecules and $n_{H_2SO_4}$ the molar quantity of absorbed sulfuric acid.

$$AU\% = \frac{m_{\text{wet}} - m_{\text{dry}}}{m_{\text{dry}}} \times 100\%, \quad (3)$$

$$AS\% = \frac{d_{\text{wet}} - d_{\text{dry}}}{d_{\text{dry}}} \times 100\%, \quad (4)$$

$$ADL = \frac{n_{\text{BI}}}{n_{\text{H}_2\text{SO}_4}}. \quad (5)$$

The acid concentration was measured by placing the blotted membrane pieces into 10 mL of 0.1 M KOH. After 24 h, the membrane pieces were washed with water and placed into 20 mL DI water. Afterwards, all solutions which had contact with the membrane were combined and titrated with 0.1 M HCl. The mass change due to the loss of chloride was considered in the calculation of the acid concentration. The additional OH^- consumption due to the ion exchange with the chloride was subtracted from the titrated OH^- consumption. Subsequently, the resulting masses of H_2SO_4 and H_2O were used to calculate the acid concentration within the membrane. Since the FAPQ330 directly turned dark red to black after immersion in an alkaline solution, acid concentration measurement was not performed.

Conductivities were measured using through-plane electrochemical impedance spectroscopy and a Zennium X provided by Zahner-Elektrik GmbH & Co. KG in a frequency range between 10 kHz and 10 MHz. A custom-made cell with two gold electrodes with an area A of $0.25 \, \text{cm}^2$ was used. For the measurement, the $1 \, \text{cm} \times 1 \, \text{cm}$ membrane pieces were soaked in $0.5 \, \text{M} \, H_2SO_4$ for 48 h. For each sample, three membrane pieces were measured. The measurements were performed within a sandwich of two $1 \, \text{cm} \times 1 \, \text{cm}$ FAPQ330 pieces to eliminate the interface resistance between the electrode and the membrane to determine R_{sample}. In addition, $R_{sandwich}$ was determined without a sample piece between the two outer FAPQ330 pieces. The interface resistance between the swollen membranes was assumed to be negligible. The resistances R were determined by taking the real part R' of the impedance when the imaginary part of the impedance R'' equals zero. The conductivity was calculated using the following equation, whereas d_{wet} is the wet thickness of the membrane piece.

$$\sigma = \frac{d_{\text{wet}}}{\left(R_{\text{sample}} - R_{\text{sandwich}}\right) \times A}. \quad (6)$$

The membrane's permeability was measured as already described in the literature using a custom-made temperature-controllable H-cell with an active area of $7.07 \, \text{cm}^2$.[51] $4 \, \text{cm} \times 4 \, \text{cm}$ membrane pieces were clamped between the two compartments. One compartment was filled with 40 mL of 1.5 M $MgSO_4$ in 3 M H_2SO_4 and the other with 40 mL of 1.5 M $VOSO_4$ in 3 M H_2SO_4. Both compartments were operated at a constant temperature (20°C) using a circulation thermostat and stirred with a magnetic stirring bar. After certain time intervals, 100 μL samples were taken from the $MgSO_4$ side. The V(IV) content was measured using a UV–Vis spectrometer (UV-1900i provided by Shimadzu, $\lambda = 764$ nm). $VOSO_4$ reference samples were removed to level the volumes on both sides of the cell. The wet thicknesses of the membranes were directly measured after disassembling the cell with the digital micrometer Series 293 from Mitutoyo. The permeability P was calculated according to the following equation: $\frac{dC_{\text{Mg},t}}{dt}$ was assigned as the slope of a linear regression model applied on the $C_{\text{Mg},t}/t$ data pairs, where t is the time and $C_{Mg,t}$ is the V(IV)-concentration on the $MgSO_4$ side at this time. C_V is the initial concentration of V(IV) on the $VOSO_4$ side, L is the wet thickness of the membrane, V_{Mg} is the initial volume on the $MgSO_4$ side, and A is the active area of the membrane.

$$P = \frac{1}{C_V} \frac{dC_{\text{Mg},t}}{dt} \frac{L V_{\text{Mg}}}{A}. \quad (7)$$

Ex-situ stability tests were performed by placing membrane pieces into 1.6 M V(V) solution in 2 M H_2SO_4 for 820 h. The V(V) solution was prepared by fully charging a 1.6 M V(III)/V(IV) solution in 2 M H_2SO_4 in an 857 Redox Flow Cell Test System from Scribner, LLC. After the test, the V(IV) concentration was measured using UV–vis spectroscopy. A blank was also tested as a baseline to account for potential V(IV) formation, which does not originate from the membrane degradation. The amount of V(IV) found in the blank sample was subtracted from the amount of V(IV) found in the sample solutions.

Tensile properties were evaluated by using the EZ Test EZ-SX provided by Shimadzu equipped with the SM-100–168,100 N force transducer from Interface Inc. Five dry $1.5 \, \text{cm} \times 4.0 \, \text{cm}$ samples were measured for each membrane at a test speed of 10 mm min^{-1}. Before the test, a preload of 0.1 N was applied, and the corresponding gauge length was subtracted from the previously measured gauge length. The Young's modulus was determined by applying a linear fit between a strain of 0.05% and 0.25%. The tensile strength was set as the stress at the maximum of the stress–strain curve. The measurements were performed at 23°C and 25% relative humidity (RH).

Electrochemical cell tests were performed at $23°C$ using a 24 cm^2 single cell comprised of 4.6 mm thermally activated carbon felts. The felts were compressed to 80%, corresponding to a 3.7 mm effective electrode thickness. Two 1 mm copper plates were used as current collectors. The measurements were performed using a flow-through design with polypropylene flow frames and graphite/polypropylene bipolar plates. 50 mL of 1.6 M V(III/IV) in 2 M H_2SO_4 on each side were precharged with a constant current (cc) of 20 mA cm^{-2} and a volume rate of 20 mL min^{-1} to state of charge (SOC) of 20% (open circuit voltage (OCV) = 1.336 V). Anolyte and catholyte were passivated with Argon throughout the entire testing procedure. Before and after any 10 cc cycles (10×50, 10×100, and 10×200 mA/cm^2), voltage–current (UI) measurements at SOC = 50% (OCV = 1.411 V) using 0, 5, 10, 20, 30, 40, 50, and 60 mA cm^{-2} were performed to derive the internal cell resistance in terms of the ASR. CEs, VEs, and EEs were determined by cycling 10 times between SOC = 20% and SOC = 80% (OCV = 1.486 V) at 50, 100, and 200 mA cm^{-2} each and using the following equations where I_d is the discharge current, I_c is the charge current, V_d is the discharge voltage, V_c is the charge voltage, and t is the time.[51] The last five cycles at each current density were used for the data evaluation.

$$CE(\%) = \frac{\int I_d dt}{\int I_c dt} \times 100\%, \qquad (8)$$

$$EE(\%) = \frac{\int V_d I_d dt}{\int V_c I_c dt} \times 100\%, \qquad (9)$$

$$VE(\%) = \frac{EE}{CE} \times 100\%. \qquad (10)$$

AUTHOR CONTRIBUTIONS

CONFLICT OF INTEREST STATEMENT
The authors have no conflicts of interest to declare.

DATA AVAILABILITY STATEMENT
The data that support the findings of this study are available from the corresponding author upon reasonable request.

ORCID
Julian Stonawski https://orcid.org/0009-0003-0062-9925
Andreas Hutzler https://orcid.org/0000-0001-5484-707X
Thomas Böhm https://orcid.org/0000-0003-2036-2159
Simon Thiele https://orcid.org/0000-0002-4248-2752
Jochen Kerres https://orcid.org/0000-0003-4972-6307

REFERENCES
[1] J. Rosamond, C. Dupont, *Polit. Governance* **2021**, *9*, 348.
[2] E. Reihani, M. Motalleb, R. Ghorbani, L. Saad Saoud, *Renew. Energy* **2016**, *86*, 1372.
[3] M. A. Basit, S. Dilshad, R. Badar, S. M. S. ur Rehman, *Int. J. Energy Res.* **2020**, *44*, 4132.
[4] Z. Huang, A. Mu, L. Wu, B. Yang, Y. Qian, J. Wang, *ACS Sustainable Chem. Eng.* **2022**, *10*, 7786.
[5] A. Z. Weber, M. M. Mench, J. P. Meyers, P. N. Ross, J. T. Gostick, Q. Liu, *J. Appl. Electrochem.* **2011**, *41*, 1137.
[6] Á. Cunha, J. Martins, N. Rodrigues, F. P. Brito, *Int. J. Energy Res.* **2015**, *39*, 889.
[7] A. Khataee, D. Pan, J. S. Olsson, P. Jannasch, R. W. Lindström, *J. Power Sources* **2021**, *483*, 229202.
[8] S. Maurya, E. Baca, K. K. Bejagam, H. Pratt, T. Anderson, R. Mukundan, C. Fujimoto, *J. Power Sources* **2022**, *520*, 230805.
[9] T. Mu, W. Tang, Y. Jin, X. Che, J. Liu, J. Yang, *ACS Appl. Energy Mater.* **2022**, *5*, 11713.
[10] J. Xu, S. Dong, P. Li, W. Li, F. Tian, J. Wang, Q. Cheng, Z. Yue, H. Yang, *Chem. Eng. J.* **2021**, *424*, 130314.
[11] D. Düerkop, H. Widdecke, C. Schilde, U. Kunz, A. Schmiemann, *Membranes* **2021**, *11*, 214.
[12] L. Gubler, *Curr. Opin. Electrochem.* **2019**, *18*, 31.
[13] B. G. Thiam, S. Vaudreuil, *J. Electrochem. Soc.* **2021**, *168*, 70553.

[14] Y. Shi, C. Eze, B. Xiong, W. He, H. Zhang, T. M. Lim, A. Ukil, J. Zhao, *Appl. Energy* **2019**, *238*, 202.

[15] M. Gigli, B. Mecheri, S. Licoccia, A. D'Epifanio, *Sustainable Mater. Technol.* **2021**, *28*, e00249.

[16] A. Ohira, W. Sakata, E. Ishida, T. Mitsuru, Y. Sato, *Int. J. Energy Res.* **2021**, *45*, 19405.

[17] L. Gubler, D. Vonlanthen, A. Schneider, F. J. Oldenburg, *J. Electrochem. Soc.* **2020**, *167*, 100502.

[18] D. Aili, J. Yang, K. Jankova, D. Henkensmeier, Q. Li, *J. Mater. Chem. A* **2020**, *8*, 12854.

[19] H. Pu, *Polym. Int.* **2003**, *52*, 1540.

[20] L. Zeng, Y. Ren, L. Wei, X. Fan, T. Zhao, *Energy Technol.* **2020**, *8*, 2000592.

[21] L. Ding, Y. Wang, L. Wang, Z. Zhao, M. He, Y. Song, *J. Power Sources* **2020**, *455*, 227965.

[22] W. Tang, Y. Yang, X. Liu, J. Dong, H. Li, J. Yang, *Electrochim. Acta* **2021**, *391*, 138919.

[23] S. Maurya, S. Diaz Abad, E. J. Park, K. Ramaiyan, Y. S. Kim, B. L. Davis, R. Mukundan, *J. Membr. Sci.* **2023**, *668*, 121233.

[24] H. E. Darling, *J. Chem. Eng. Data* **1964**, *9*, 421.

[25] M. Jung, W. Lee, C. Noh, A. Konovalova, G. S. Yi, S. Kim, Y. Kwon, D. Henkensmeier, *J. Membr. Sci.* **2019**, *580*, 110.

[26] R. S. Bhavsar, S. C. Kumbharkar, U. K. Kharul, *J. Membr. Sci.* **2012**, *389*, 305.

[27] V. Jovanovski, R. Marcilla, D. Mecerreyes, *Macromol. Rapid Commun.* **2010**, *31*, 1646.

[28] A.-L. Pont, R. Marcilla, I. de Meatza, H. Grande, D. Mecerreyes, *J. Power Sources* **2009**, *188*, 558.

[29] Y. Gerchman, B. Vasker, M. Tavasi, Y. Mishael, Y. Kinel-Tahan, Y. Yehoshua, *Bioresources Technol.* **2017**, *228*, 141.

[30] Y. Wang, S. Wang, M. Xiao, D. Han, M. A. Hickner, Y. Meng, *RSC Adv.* **2013**, *3*, 15467.

[31] Z. Tao, C. Wang, S. Cai, J. Qian, J. Li, *ACS Appl. Energy Mater.* **2021**, *4*, 14488.

[32] T. Itaya, H. Ochiai, T. Aoyama, K. Ueda, A. Imamura, *J. Polym. Sci. B: Polym. Phys.* **1994**, *32*, 171.

[33] E. Bülbül, V. Atanasov, M. Mehlhorn, M. Bürger, A. Chromik, T. Häring, J. Kerres, *J. Membr. Sci.* **2019**, *570-571*, 194.

[34] H. Cho, V. Atanasov, H. M. Krieg, J. A. Kerres, *Polymers* **2020**, *12*, 915.

[35] M. T. Tsehaye, X. Yang, T. Janoschka, M. D. Hager, U. S. Schubert, F. Alloin, C. Iojoiu, *Membranes* **2021**, *11*, 367.

[36] A. Fdz De Anastro, N. Lago, C. Berlanga, M. Galcerán, M. Hilder, M. Forsyth, D. Mecerreyes, *J. Membr. Sci.* **2019**, *582*, 435.

[37] C. K. Ober, G. Wegner, *Adv. Mater.* **1997**, *9*, 17.

[38] D. Valade, F. Boschet, S. Roualdès, B. Ameduri, *J. Polym. Sci., Part A: Polym. Chem.* **2009**, *47*, 2043.

[39] L. Hager, M. Hegelheimer, J. Stonawski, A. T. S. Freiberg, C. Jaramillo-Hernández, G. Abellán, A. Hutzler, T. Böhm, S. Thiele, J. Kerres, *J. Mater. Chem. A* **2023**, *11*, 22347.

[40] Y. W. Guo, W. W. Cui, W. H. Xu, Y. Jiang, H. H. Liu, J. Y. Xu, Z. Q. Gao, L. Z. Liu, *Adv. Mater. Res.* **2014**, *981*, 891.

[41] M. Mara Ikhsan, S. Abbas, X. H. Do, S.-Y. Choi, K. Azizi, H. A. Hjuler, J. H. Jang, H. Y. Ha, D. Henkensmeier, *Chem. Eng. J.* **2022**, *435*, 134902.

[42] F. Arslan, K. Chuluunbandi, A. T. S. Freiberg, A. Kormanyos, F. Sit, S. Cherevko, J. Kerres, S. Thiele, T. Böhm, *ACS Appl. Mater. Interfaces* **2021**, *13*, 56584.

[43] S.-Y. Choi, S. Cho, D. Kim, J. Kim, G. Song, R. Singh, C. Kim, *J. Membr. Sci.* **2021**, *620*, 118904.

[44] C. Noh, M. Jung, D. Henkensmeier, S. W. Nam, Y. Kwon, *ACS Appl. Mater. Interfaces* **2017**, *9*, 36799.

[45] Z. Zhao, Q. Dai, X. Li, S. Zhang, S. Li, X. Li, *J. Mater. Chem. A* **2022**, *10*, 762.

[46] B. Zhang, Q. Wang, S. Guan, Z. Weng, E. Zhang, G. Wang, Z. Zhang, J. Hu, S. Zhang, *J. Power Sources* **2018**, *399*, 18.

[47] K.-D. Kreuer, A. Münchinger, *Annu. Rev. Mater. Res.* **2021**, *51*, 21.

[48] B. Dey, M. W. Ahmad, A. ALMezeni, G. Sarkhel, D. S. Bag, A. Choudhury, *Compos. Commun.* **2020**, *17*, 87.

[49] K. Geng, H. Tang, Q. Ju, H. Qian, N. Li, *J. Membr. Sci.* **2021**, *620*, 118981.

[50] J. Lobato, P. Cañizares, M. A. Rodrigo, J. J. Linares, J. A. Aguilar, *J. Membr. Sci.* **2007**, *306*, 47.

[51] H. Zhang, X. Li, J. Zhang Eds., *Redox flow batteries: Fundamentals and applications*, CRC Press/Taylor & Francis Group, Boca Raton **2018**.

SUPPORTING INFORMATION

Additional supporting information can be found online in the Supporting Information section at the end of this article.